Physical Gelation of Gelatin Studied with Rheo-Optics

Liang Guo,[†] Ralph H. Colby,*[,†] Charles P. Lusignan,[‡] and Andrew M. Howe[§]

Materials Science and Engineering, The Pennsylvania State University, University Park, Pennsylvania 16802, Imaging Materials and Media, R&D, Eastman Kodak Company, Rochester, New York 14650-2109, Kodak Limited R&D, Headstone Drive, Harrow, Middlesex, HA1 4TY, U.K.

Received February 28, 2003; Revised Manuscript Received September 26, 2003

ABSTRACT: A rheo-optical device outfitted with a Peltier temperature control for rapid temperature changes has been constructed that allows simultaneous measurement of the optical rotation of light and the controlled-stress rheology. Optical rotation provides a direct in situ assessment of the extent of triple helix reversion in a gelatin solution undergoing physical gelation in the rheometer. Thermal gelation of gelatin was monitored over a wide range of concentrations and temperatures. Assuming dynamic scaling theory applies, viscosity data below the gel point were used to evaluate the gel point and determine the value of the viscosity exponent. Above the gel point, creep-recovery experiments are used to measure the shear modulus and determine the dynamic scaling elastic modulus exponent. During thermal gelation, the time-dependent optical rotation shows an initial rapid growth region where new helices are formed, followed by a slower growth region involving helix lengthening. For cases where the gel point occurs before the helix reversion slows appreciably, the viscosity and modulus exponents are found to depend on gelatin concentration, but not on temperature. However, anomalous exponents are measured using the same methods at higher temperatures, where the helix reversion slows appreciably before the gel point is reached. These results suggest that extreme caution must be used in evaluating dynamic exponents from any physical gelation process. The observed concentration dependences of the dynamic scaling exponents are discussed in terms of chain overlap and entanglement. For gelatin gelation, the plethora of different, reported percolation exponents in the literature are rationalized.

Introduction

Gelatin is a polypeptide made by hydrolytic degradation of collagen and is widely used in food, pharmaceutical, and photographic industries. Since this biopolymer owes many of its uses to its coil−helix transition, study of this physical gelation process has attracted considerable research attention for over 50 years.[1−7]

The native conformation of collagen molecules is a triple helix formed by three individual molecular strands held together by interchain hydrogen bonding.[8] Gelatin is denatured collagen and dissolves in water at temperatures above the melting temperature, existing as flexible individual coils in solution. On cooling below the melting temperature, ordered structures of the gelatin molecules are reformed. X-ray diffraction,[9] scattering,[10] and transmission electron microscopy[11] measurements strongly suggest that the reconstructed, ordered structures have the same conformation as collagen. Gelatin molecules partially revert to the ordered helical collagen-like sequences, separated along the gelatin molecular contour by peptide residues in the disordered coil conformation. While the coil−helix reversion is predominantly intramolecular through a back refolding of the single chains at very low concentrations $c \sim 0.01-0.1$ wt %,[3] it becomes increasingly intermolecular as concentration is raised and leads to gelation at concentrations above 0.5−1.0 wt %[12] caused by the formation of an infinite network of intermolecularly connected molecules in the gelatin solution.

Percolation theory describes the structural evolution of branched molecules connected intermolecularly (physically or chemically) at random.[13] Gelation in polymer systems, either chemical or physical, can be described by bond percolation theory. The probability that bonds are formed between molecules is called the bond fraction p. Bonds between gelatin molecules take the form of triple helices, and the bond fraction in this system is proportional to the number of triple helices per gelatin molecule at a given time. The system changes from a viscoelastic liquid to a viscoelastic solid when a critical number of helices or, more generally, bonds, per molecule p_c have formed. At this point, a molecule of macroscopic size (the gel or network) coexists with, and is swollen by, the remaining branched molecules of finite size (the sol). At the gel point p_c, the solution viscosity, the weight-average and z-average molar mass, and the correlation length all diverge.[13]

Analogous to second-order phase transitions, gelation in polymer systems is a continuous phase transition in molecular connectivity. Physical quantities diverge at the gel point p_c as power laws in the relative extent of reaction:

$$\epsilon = (p - p_c)/p_c \tag{1}$$

A value of $\epsilon < 0$ indicates that the system is below the gel point, while a value of $\epsilon > 0$ shows that the system is above the gel point. The viscosity below the gel point diverges as the gel point is approached (as $\epsilon \rightarrow 0$)

$$\eta = A(-\epsilon)^{-s} \quad \text{for} \quad p < p_c \quad \text{or} \quad \epsilon < 0 \tag{2}$$

Above the gel point, the equilibrium shear modulus of the network grows steadily from a value of zero at the gel point

* Corresponding author. E-mail: rhc@plmsc.psu.edu.
† The Pennsylvania State University.
‡ Eastman Kodak Co.
§ Kodak Limited R&D.

10.1021/ma034266c CCC: $25.00
Published on Web 11/26/2003

$$G_e = B\epsilon^t \quad \text{for} \quad p > p_c \quad \text{or} \quad \epsilon > 0 \tag{3}$$

Prefactors A and B in eqs 2 and 3 have the same units as viscosity and modulus, respectively. The validity of the scaling description for rheological properties observed during the thermodynamically driven sol−gel transition of gelatin solutions has been well documented by experimental studies.[4,6,14−17] Theories based on different assumptions, predict different values for the exponents s and t. Experiments under different conditions, also give diverse values for the exponents. Some typical values found in the literature for the exponents s and t are given in Table 1. The relaxation exponent u is defined[18−20] for the stress relaxation modulus at the gel point

$$G(t) = St^{-u} \tag{4}$$

The relaxation exponent u is related to s and t by dynamic scaling[21−23]

$$u = \frac{t}{s+t} \tag{5}$$

The particular molecular architecture of each individual system plays an important role in affecting the critical exponents. In this paper, we report our systematic experimental studies of the physical gelation of aqueous gelatin solutions at different concentrations and temperatures. We find that the exponents are functions of concentration.

Experiment

Deionized lime-processed bovine ossein gelatin of molecular weight 118 kDa in granules (SKW Gelatin and Specialties) was used as received without further purification. The only appreciable salt came from a pH adjustment with NaOH which typically amounted to about 3000−3500 ppm sodium in the gelatin. All other anions and cations were less than 100 ppm. The solution pH of this gelatin was 5.7−5.8 and the isoelectric point of this gelatin is 4.9. The gelatin contained 13.47% moisture by weight, and the dry gelatin density was determined to be 1.45 g/cm^3 by measuring the weight of an aqueous gelatin solution of known concentration and volume. Aqueous gelatin solutions were prepared by swelling the gelatin in distilled, deionized water at room temperature for 1 h, followed by subsequent heating at 45 °C for another hour under constant agitation by mild shaking. Concentration is based on dry gelatin weight and Kathon biocide (Rohm and Haas) was added as an antibacterial agent to the solutions at the level of 0.2 g/dL. No pH adjustment was made to the gelatin solutions, and the prepared solutions were stored in a refrigerator at 5 °C until use. The concentration of gelatin for this study is quoted as g/dL at room temperature of ∼23 °C. The water volume change is less than 1% for the complete quenching temperature range (45−10 °C) of our study.

Gelatin is an optically active material in both the random coil and helix conformations as a result of the chiral centers on the molecule, but has more optical activity in the helix state. The polarization of an incident polarized light beam passing through the gelatin sample will be rotated an angle α, depending on the beam wavelength and the optical activity. The optical rotation, α (in degrees), measured at beam wavelength, λ, is normalized by the beam path length, l (in decimeters), and the gelatin concentration c (in grams per deciliter) to yield the specific optical rotation:

$$[\alpha]_\lambda = \frac{100\alpha}{lc} \tag{6}$$

The optical rotation of a gelatin sample is related to the fraction of renatured (reconstructed) triple helices. Assuming a linear relationship between optical rotation and the fraction of gelatin in the triple helix state, the following formula is readily derived for the fraction of gelatin in the triple helix conformation[37]

$$X = \frac{[\alpha]_\lambda - [\alpha]_\lambda^{\text{coil}}}{[\alpha]_\lambda^{\text{collagen}} - [\alpha]_\lambda^{\text{coil}}} \tag{7}$$

where $[\alpha]_\lambda^{\text{coil}}$ is the specific rotation of the sample at a given quench temperature, if all the molecules are in the coil state, and $[\alpha]_\lambda^{\text{collagen}}$ is the specific rotation (considered as temperature independent), if all the molecules are in the triple helix conformation (the native state of collagen).

Assuming that the bond fraction is proportional to the helix fraction $p \propto X$ for a given gelatin system (i.e., the average bond length does not change with time, though it may be different at different concentrations and temperatures), the relative extent of reaction (eq 1) can be rewritten as

$$\epsilon = (X - X_{\text{gel}})/X_{\text{gel}} = ([\alpha]_\lambda - [\alpha]_\lambda^{\text{gel}})/([\alpha]_\lambda^{\text{gel}} - [\alpha]_\lambda^{\text{coil}}) \tag{8}$$

where $[\alpha]_\lambda^{\text{gel}}$ and X_{gel} are the specific optical rotation and the helix fraction at the gel point, respectively. Physical gelation of gelatin is one of the rare cases for which the extent of reaction ϵ can be determined very precisely and nondestructively during the gelation process from polarimetry measurements. Hence, simultaneous measurement of optical rotation and rheology allows direct testing of eqs 2 and 3. Notice, also, that the optical rotation of the purely helical state $[\alpha]_\lambda^{\text{collagen}}$ does not enter into the relative extent of reaction ϵ.

However, to calculate the fraction of renatured helices from eq 7, both $[\alpha]_\lambda^{\text{collagen}}$ and $[\alpha]_\lambda^{\text{coil}}$ must be known. The wavelength dependence of the specific optical rotation of collagen and gelatin at wavelength $\lambda > 300$ nm has been shown to follow the Drude equation[38]

$$[\alpha]_\lambda = D\frac{{\lambda_0}^2}{\lambda^2 - {\lambda_0}^2} \tag{9}$$

where the factor D depends on the conformation of the protein, and λ_0 is the wavelength of the absorption maximum. The literature value of λ_0 for both gelatin and collagen is $\lambda_0 = 212$ nm,[5] and the literature value of $[\alpha]_\lambda^{\text{collagen}}$ for limed ossein[5] is $[\alpha]_{436}^{\text{collagen}} = -800 \pm 10$ (the levorotary optical rotation of gelatin is negative by definition). Our optical rotation measurements were performed at a wavelength of $\lambda = 632.8$ nm and the corresponding specific optical rotation of collagen is calculated according to eq 9:

$$[\alpha]_{632.8}^{\text{collagen}} = -327 \pm 5$$

Our separate kinetics study[39] shows that the temperature dependent $[\alpha]_{623.8}^{\text{coil}}$ can be expressed as

$$[\alpha]_{632.8}^{\text{coil}} = 0.311T - 134$$

where temperature T is in Celsius.

To simultaneously measure the rheology and optical rotation of the gelatin solutions during thermal gelation, we built a rheo-optical device that combines a Rheometrics controlled-stress rheometer, a polarimeter, and a Peltier temperature controller. A sample cell was fabricated and placed on top of the Peltier temperature controller as shown in Figure 1. The cell includes an acrylic cup with two fused silica windows and an acrylic top plate with diameter 53.34 mm. An acrylic cover, with a thermal shielding layer on its inner wall, was used for thermal insulation. For each experiment, a vial containing the gelatin gel was taken from the refrigerator and heated to 45 °C until the gel was completely melted. The liquid sample was

Table 1. Theoretical Predictions and Experimental Observations for the Rheological Exponents Associated with the Sol−Gel Transition

	s	*t*	*u*	ref
		Theoretical Predictions		
classical mean field	0	3	1	24−26
electrical analogy	0.75	1.9	0.72	27, 28
Rouse model	1.3	2.6	0.67	21, 29
vector percolation		3.5−4		30
		Experimental Chemical Gels		
silica gels	0.8−1.3	2.2−2.6	0.7−0.72	31, 32
epoxy	1.4		0.63−0.7	21, 28, 33
polyester without interchain entanglement	1.36	2.7	0.66	34
polyester with interchain entanglement	6.1	3.2	0.33	35
		Experimental Physical Gels		
gelatin	1.5	1.8−2.0	0.2−0.7	6, 7, 16
pectin	0.82	1.9	0.71	15
PVC in bis(2-ethylhexyl) phthalate	1.5	2.6	0.75	36

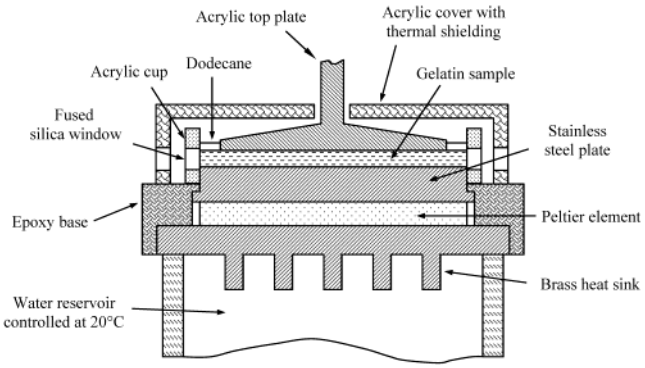

Figure 1. Schematic of the sample cell, rheometer fixture, solvent trap, and Peltier temperature controller assembly.

transferred quickly to the sample cell to minimize water evaporation. The top plate was set to a gap of 2.5 mm to allow the entire laser beam to transmit through the sample. The sample surface between the wall of the cup and the edge of the top plate (Figure 1) was covered with dodecane to minimize water evaporation (part of the inclined upper surface of the top plate was also covered).

The Peltier temperature controller consisted of a stainless steel plate with an RTD (resistance temperature device) thermal sensor sitting in a small aperture beneath it, a Peltier thermal element, and a comblike brass heat sink with its comb teeth immersed in a small water bath. The small water bath was connected to a separate circulating water bath with its temperature set at 20 °C. The Peltier element was driven by a KEPCO model BOP 15−20 bipolar operational power amplifier with an output capability of ±15 V and ±20 A. Temperature sensing and the power supply for the Peltier temperature controller were fully automated by interfacing with a National Instrument DAQ board in a computer running our LabVIEW code. A temperature ramp as fast as 20 K/min was achieved, and the final temperature was stabilized within ±0.1 K.

The polarimeter (Figure 2) was built[40] using a He−Ne laser source of wavelength 632.8 nm, two polarizers, a photoelastic modulator (PEM) and controller (model PEM-90, Hinds Instruments), a detector, and a lock-in amplifier (model SR810 DSP, Stanford Research Systems). With a chosen retardation (usually in the range between half- and quarter-wavelength of the laser beam) and modulation frequency, *f*, for the photoelastic modulator, the ratio of the 2*f* component in the signal, to the DC component of the signal, is directly related to the optical rotation α by

$$\frac{V_{2f}}{V_{dc}} = \frac{C_1 \sin(2\alpha)}{1 + C_2 \sin(2\alpha)} \tag{10}$$

where V_{2f} and V_{dc} are the voltage of the 2f and dc components of the signal on the detector, and the constants C_1 and C_2

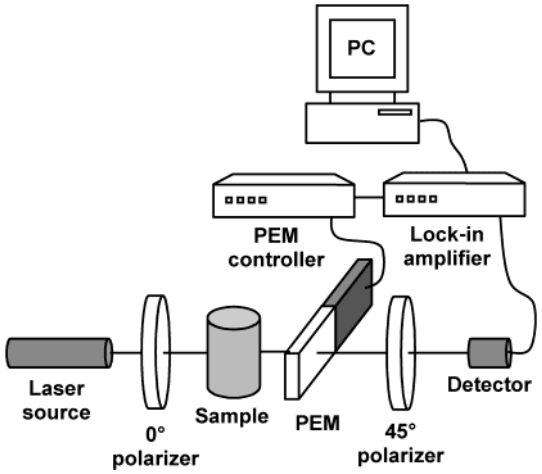

Figure 2. Diagram of polarimeter optical train and electronics.

depend on retardation and need to be determined by calibration. The derivation of eq 10 is given in Appendix I, and the reader is referred to Fuller[41] for the fundamentals of the optical rheometry technique. The polarimeter was calibrated by rotating the first polarizer with the resulting ratio V_{2f}/V_{dc} calculated by the lock-in amplifier. The calibration was checked with optical rotation standards (L-proline and L-alpha-bromocamphor-π-sulfonic acid, ammonium salt). Our polarimeter can detect a rotation angle α as small as 0.001°.

At the start of an experiment, the gelatin solution in the sample cell was maintained at 45 °C for 1000 s. This time was found to be sufficient for eliminating thermal history effects in the gelatin sample. Next, it was quenched to the desired gelation temperature (at the system maximum ramp rate of 20 K/min). Rheology and optical rotation data were acquired simultaneously. Below the gel point, a constant small stress was applied, and the shear strain was recorded as a function of time. Viscosity was calculated from the local slope of the time-dependent strain. The small stress used was in the range ∼1−8 dyn/cm^2, depending on the solution concentration. We verified that the small stress used for the viscosity measurement did not cause alignment of gelatin molecules, which may introduce linear birefringence and affect the optical rotation measurement. We also verified that the stress level chosen had minimal effect on the viscosity results (as demonstrated in Figure 3); therefore all the viscosity data are very close to the zero-shear rate limit. Huang and Sorensen's viscosity measurements,[43] on a gelatin solution (3 wt %) quenched to 28 °C, demonstrate that when the shear rate is switched to a lower value at different times after quench, all the high-shear-rate viscosity vs time curves converge to the one at the lower shear rate. Thus, the viscosity of gelatin solutions during gelation does not depend on shear rate history and small shear stresses do not affect helix formation, so the bond fraction *p*

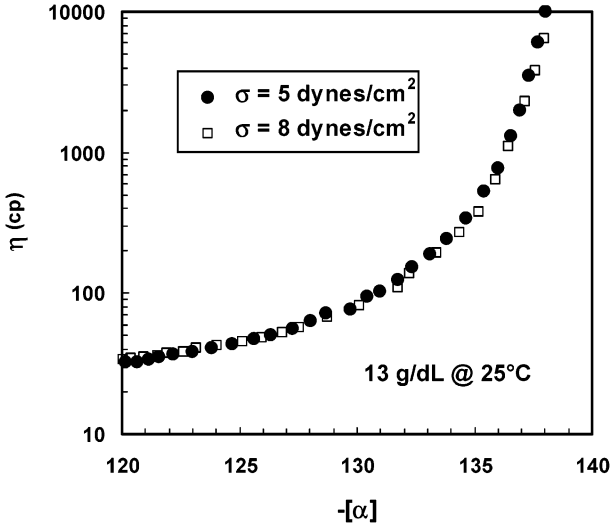

Figure 3. Viscosity measured at different applied stress levels plotted against optical rotation for a 13 g/dL gelatin solution quenched to 25 °C. Identical curves indicate that both applied stress levels are in the zero shear rate viscosity regime.

is not a function of shear rate. This conclusion is confirmed by our polarimetry measurements in which the applied shear has no effect on the optical rotation *before the gel point*. However, gelatin solutions do exhibit shear thinning during gelation. The main advantage of using controlled-stress rheology to study gelation is that, at a constant low shear stress, the plate rotation slows down as the gel point is approached because of the large increase in viscosity. Reliable viscosity data corresponding to zero shear rate can be obtained very close to the gel point without affecting the bond fraction p. This allows precise location of the gel point by fitting the measured data to eq 2.

Creep and recovery experiments were performed to measure the shear modulus beyond the gel point. According to the gel modulus level, a particular stress level was chosen to ensure that the shear strain was in the range from 0.003 to 0.01. The stress could be as low as 0.5 dyn/cm^2 for low concentrations slightly above the gel point and as high as 150 dyn/cm^2 for high concentrations far beyond the gel point. Unfortunately, the large stress, which was necessary for a gel of relatively high modulus developed far beyond the gel point, aligned the gelatin molecules and caused stress-induced linear birefringence that was evident in the apparent optical rotation. However, because the linear birefringence disappeared when the stress was released, the optical rotation just after the start of the recovery curve could be used, and the corresponding modulus was calculated from the recovery curve for all the experiments (see Figure 4). Modulus measurements close to the gel point were not possible because the relaxation times were too long, as will be discussed in detail below. In all cases, the relative extent of reaction range $0.1 < \epsilon < 1$ was accessed for the determination of the exponent t in eq 3.

Viscosity of gelatin solutions in the coil state was measured at 45 °C with a Bohlin CS50 controlled-stress rheometer using a C2.3/26 bob-and-cup geometry in the low-shear rate regime and an Anton Paar AMVn rolling ball viscometer.

The relaxation exponent u at the gel point was measured at a constant strain of 0.01 with the Bohlin CS50 or CVO120 controlled-stress rheometers thermostated with a water jacket surrounding the measuring cup. The u value was determined by finding the frequency independent loss angle δ at the gel point (the dynamic moduli scale as $G' \propto G'' \propto \omega^u$)[18−20,42]

$$u = \frac{2\delta}{\pi} = \frac{2}{\pi}\tan^{-1}\left(\frac{G''}{G'}\right) \qquad (11)$$

Remelting experiments were also performed to study the helical structure of the gel. A gelatin solution was quenched and stabilized at a low temperature for a certain time and the temperature was raised at a constant heating rate. Gelatin gelation is a nonequilibrium process, as shown by the fact that the network never stops developing.[5] Thus, the heating rate for remelting must be faster than the rate of helix formation. Conversely, heating at too fast a rate creates a thermal lag and inaccuracy in the remelting curve determination. Practically, an optimal heating rate must be chosen that minimizes both helix growth rate and thermal lag. For example in our measurements, a heating rate of 2 K/min was used for remelting a sample near the gel point for a 1.51 g/dL solution quenched to 15 °C, and a heating rate of 0.5 K/min was used for a 5.08 g/dL solution quenched to 25 °C. Far beyond the gel point, a heating rate as low as 0.05 K/min could be used as a result of the slowing down of the helix growth. However, heating rates lower than 0.05 K/min would allow the melted helix to recrystallize during heating.

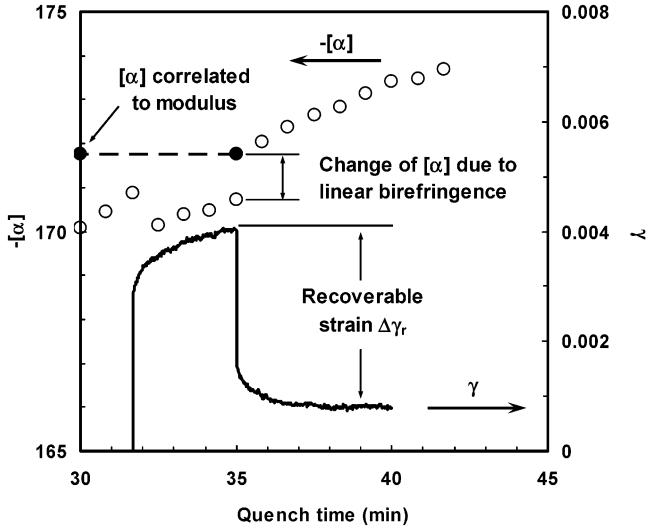

Figure 4. Time evolution overlay plot displaying the creep-recovery curve at a stress of $\sigma = 35$ dyn/cm^2 and the corresponding optical rotation for a 10.3 g/dL gelatin solution quenched to 25 °C. The recoverable strain $\Delta\gamma_r$ determines the modulus $G_e = \sigma/\Delta\gamma_r$. The interpolated optical rotation data point (filled circle) from the measured ones (open circles) is used as the optical rotation corresponding to the modulus. Note the optical rotation change as a result of linear birefringence induced by the applied stress.

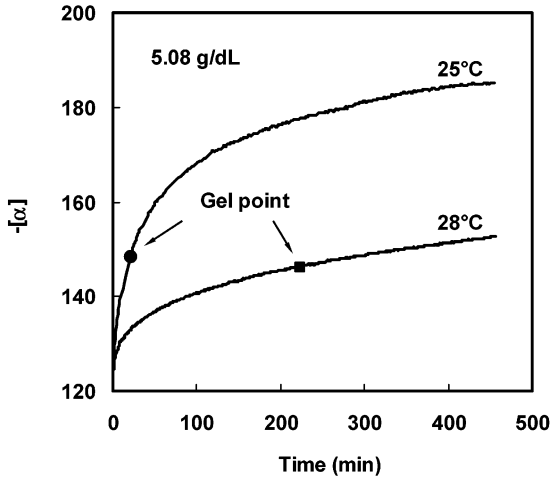

Figure 5. Specific optical rotation of a 5.08 g/dL gelatin solution quenched to 25 and 28 °C.

Results

Optical Rotation During Gel Formation and Remelting. Figure 5 shows the time-dependent specific rotation for 5.08 g/dL gelatin in water after quenching

to 25 and 28 °C. The specific optical rotation is negative because gelatin is levorotatory. The magnitude of the specific rotation has an initial jump from $[\alpha]_{632.8} = -120°$ at 45 °C to the value in the coil state at the quench temperature, $[\alpha]_{632.8}^{coil}$, and then continuously increases with time, indicating a continuous increase of triple-helix content, over time, in the sample at the quench temperature. The gelation process can be divided into two distinctive stages: an initial fast helix growth immediately after quenching and a long period thereafter with a slow helix growth rate. Djabourov and co-workers[5] have proposed that the formation of a loose network caused by the nucleation of several helical segments on each chain corresponds to the first fast process of helix growth, and the second process should be a slow reorganization of this network striving to reach the equilibrium state of full renaturation (collagen). Although the first fast nucleation process is a familiar idea borrowed from polymer crystallization, the second slow reorganization, or helix extension process, needs experimental proof. To the best of our knowledge, our following remelting measurements provide *the first direct experimental verification of this idea*. The symbols on the optical rotation curves in Figure 5 indicate the location of the gel point, whose determination will be discussed later in the following section on viscosity. The time required to reach the gel point, relative to the transition time between the fast and slow processes, will prove central for understanding the exponents obtained from experiments for gelatin solutions.

Helices formed after quenching, remelt again when temperature is raised. The specific rotation curve recorded in the remelting process contains information about the helix fraction that has a certain melting temperature (or, equivalently, a certain helix length). The melting temperature equation of a polymer can be adapted to describe the remelting of gelatin triple helices

$$T_m = T_m^0\left(1 + \frac{2\sigma_e}{l\Delta H}\right) \tag{12}$$

where T_m is the melting temperature of a triple helix of length l, T_m^0 is the equilibrium melting temperature at infinite helix length, ΔH (<0) is the enthalpy change per helix length when the helix is formed, and $2\sigma_e$ is the interfacial free energy at the two ends of the helix. The significance of eq 12 is that *helices of different lengths have different melting temperatures, with longer helices melting at higher temperatures.*

Differentiation of eq 7, with respect to temperature yields

$$\frac{dX}{dT} = \frac{d}{dT}\left(\frac{[\alpha] - [\alpha]_{632.8}^{coil}}{[\alpha]_{632.8}^{collagen} - [\alpha]_{632.8}^{coil}}\right)$$

$$= \frac{d}{dT}\left(\frac{[\alpha] - 0.311T + 134}{-193 - 0.311T}\right) \tag{13}$$

A plot of dX/dT vs temperature T specifies the volume fraction distribution of helices as a function of melting temperature or helix length (see eq 12). Parts a and b of Figure 6 show the remelting curves and their temperature derivative (the volume fraction distribution) for a 5.08 g/dL gelatin sample that has been quenched

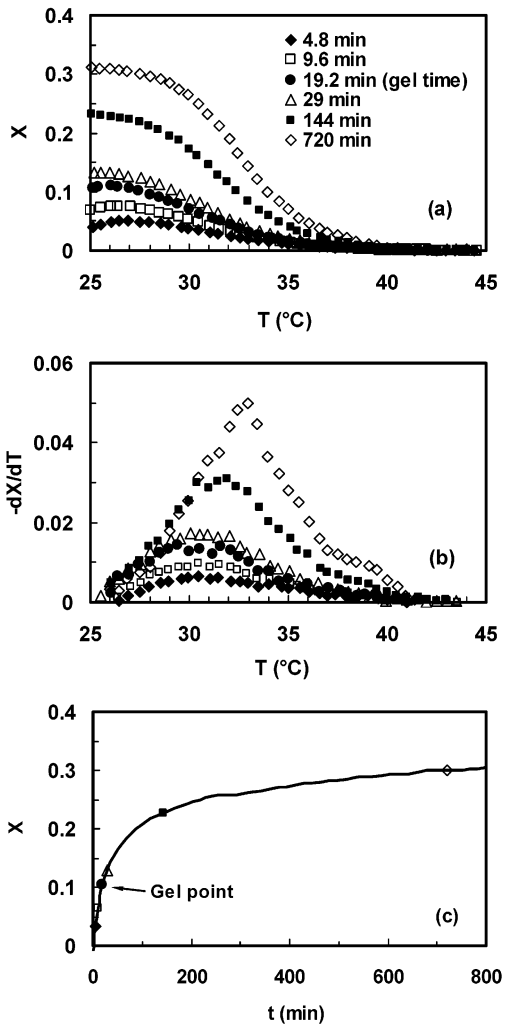

Figure 6. Remelting curves (a) and their derivatives (b) for a 5.08 g/dL gelatin solution quenched to 25 °C for different times. The heating rate is 0.5 K/min. The times at which remelting data were taken are shown as the symbols in part c.

to 25 °C for different times. During the early stage after quenching, the distribution curve of helix lengths simply increases in magnitude, indicating that helices of the same length are being formed, and their number density increases with time. The distribution curve shifts to higher temperature at long times, suggesting that the helices extend their length gradually. There may be new helices formed at long times, but the extension of the existing helices is the main feature, as demonstrated by the *decrease* of the distribution curve at the low temperature end. Figure 6c shows the points on the helix growth curve where each remelting measurement was taken. During the fast increase stage before the "knee" of the helix growth curve, the helix length does not change, while after the "knee," the helices gradually increase in length. Figure 6c also shows that gelatin at a concentration of 5.08 g/dL and a temperature of 25 °C reaches the gel point before the knee, implying a linear relation between bond fraction p and optical rotation α. However, remelting experiments done at 28 °C indicate that the 5.08 g/dL gelatin solution reaches the gel point beyond the knee (see Figure 5). A linear relationship between p and α does not hold in this situation because of helix lengthening, and the rheological exponents determined by forced fitting to dynamic scaling laws will be meaningless. The tempera-

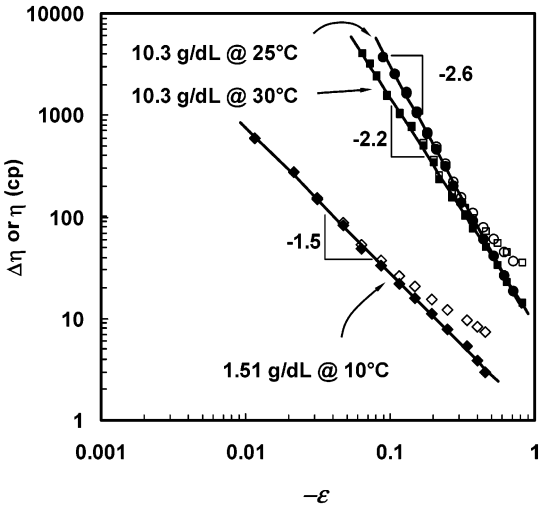

Figure 7. Viscosity of gelatin solutions fitted to both $\eta = A|\epsilon|^{-s}$ and $\Delta\eta = A|\epsilon|^{-s}$ with ϵ given by eq 8. This technique provides the most accurate estimate of the gel point in terms of a critical specific rotation: $[\alpha]^{gel} = 185.7$ for 1.51 g/dL gelatin quenched to 10 °C and $[\alpha]^{gel} = 140.5$ and 138.2 for 10.3 g/dL gelatin quenched to 25 and 30 °C, respectively. Filled symbols are for the viscosity change ($\Delta\eta$) and open symbols are for the viscosity (η).

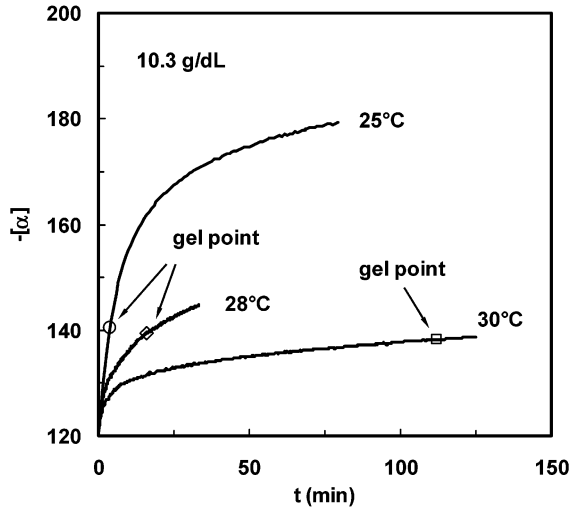

Figure 8. Optical rotation as a function of time for a 10.3 g/dL gelatin solution quenched to three different temperatures as indicated in the figure. When the gel point moves beyond the "knee" on the optical rotation curve, the linear relationship between optical rotation and the bond fraction is no longer valid.

ture T_l at which the gel point coincides with the knee position is the maximum temperature where a linear relationship between p and α can still be valid. For the 5.08 g/dL gelatin solution, T_l is between 25 and 28 °C.

Viscosity Below the Gel Point. Viscosity and optical rotation were measured simultaneously for gelatin solutions at different temperatures and concentrations. A plot of viscosity against optical rotation for a 13 g/dL gelatin solution quenched to 25 °C is shown in Figure 3. The viscosity data were fitted to eqs 2 and 8 to determine the viscosity scaling exponent. Two fitting methods were used to test the applicability of the scaling ideas. One was to fit the viscosity η directly to eq 2, using the optical rotation at the gel point $[\alpha]^{gel}_{632.8}$, the exponent s and the prefactor A as adjustable parameters. The second method uses the same three-parameter fitting procedure with the change in viscosity $\Delta\eta = \eta - \eta_0$ replacing the viscosity η in eq 2, where η_0 is the initial solution viscosity immediately after quenching. Figure 7 demonstrates the results of the two fitting approaches for 1.51 and 10.3 g/dL gelatin solutions quenched to different temperatures. The viscosity change $\Delta\eta$ approach fits the dynamic scaling model over a wider range in ϵ, with the same power law exponent s observed *close* to the gel point as when the solution viscosity η is analyzed.

The different slopes observed in Figure 7 indicate that dynamic scaling applies for thermal gelatin gelation but that solutions with different concentrations have different values of the exponent s. To further complicate the issue, different s values are obtained at different temperatures for solutions with the same gelatin concentration. By examining the location of the gel point on the optical rotation curves as shown in Figure 8, we conclude that the apparent temperature dependence of the exponent s is the result of helix length change. The gel point at 25 °C is in the fast-growth region and the exponent $s \approx 2.6$. The gel point at 28 °C is around the knee, separating the fast- and slow-growth regions. The gel point at 30 °C is far beyond the knee. The apparent exponent $s \approx 2.1$ at 28 and 30 °C is lowered due to the fact that significant helix lengthening occurs before the gel point is reached.

Table 2 lists the experimental values determined for the exponents s and t, and also the optical rotation $[\alpha]^{gel}$ at the gel point for gelatin solutions of different concentrations quenched to different temperatures. The values listed in *italics* are for circumstances where the gelatin solutions reach the gel point in the *slow* helix growth region beyond the "knee," where the fitted exponent values are suspect. The determination of the exponent t for the modulus will be described in the next section. Compared to the results in Table 2, a 4.7 wt % gelatin sample studied by Djabourov and co-workers[6] has a lower exponent $s = 1.48$ when quenched to 27.5 °C, because the sample reaches the gel point beyond the knee.

As we have defined above, T_l is the temperature at which the gel point coincides with the knee location. For any temperature above T_l, the gel point will be beyond the knee and a linear relationship does not hold between the bond fraction p and optical rotation α. Consequently, meaningful scaling exponents cannot be extracted from the data obtained above T_l. Quenching a gelatin solution to a temperature below T_l ensures fast helix formation in the system so that the gel point is reached before the knee. T_l corresponds to a characteristic helix formation rate that is universal for all gelatin concentrations. Assuming that a constant second-order (concentration dependence) reversion rate determines T_l (see Appendix II for details), one finds

$$T_l(K) = (35 + 0.18c_0 + 273)\left(1 - \frac{0.28}{2\ln c_0 + 5.06}\right) \quad (14)$$

where c_0 is the initial concentration of gelatin (in g/dL). The solid line in Figure 9 is the concentration-dependent T_l curve, calculated according to eq 14. The data points with error bars are estimates of T_l, made according to Table 2. Also shown in Figure 9 is the sol−gel transition temperature T_{gel} determined by Michon and co-workers.[16] A system gels when quenched to a temperature below T_{gel}, but gelation never occurs if the quench temperature is above T_{gel}. Below T_l, the gel point occurs

Table 2. Critical Exponents, Optical Rotation at the Gel Point and Prefactors for Gelatin Solutions Quenched to Different Temperatures as Determined by the Scaling Laws $\Delta\eta = A(-\epsilon)^{-s}$ and $G_e = B\epsilon^t$ [a]

C (g/dL)	T (°C)	-[α]^{gel} (deg)	s	A (cp)	t	B (dyn/cm^2)	C (g/dL)	T (°C)	-[α]^{gel} (deg)	s	A (cp)	t	B (dyn/cm^2)
1	10	216.1	1.1	1.1			7.68	22.5	144.2	2.3	4.6		
	15	207.2	1.34	0.93				25	142.4	2.46	3.3		
	15	206.9	1.35	0.72				25	142.9	2.4	4.7		
	20	*196.3*	*1.5*	*0.55*				28	*141.4*	*1.66*	*5.4*		
1.51	10	185.9	1.5	0.93	2.45	1300	10.3	25	140.5	2.6	7.2	1.6	3400
	10	185.7	1.45	0.86				25	140.4	2.6	8.5		
	15	182.3	1.45	0.95	2.3	960		28	*138.7*	*2.1*	*11*	*1.84*	
	15	181.9	1.3	1.2				28	*139.0*	*2.0*	*12*		
	20	178.3	1.4	0.97	2.26	1200		30	*138.2*	*2.2*	*9.0*	*2.6*	
	20	178.6	1.4	0.98				30	*137.1*	*1.8*	*11*	*2.8*	
2.62	15	162.0	1.84	0.70	2.16	930	13	25	140.0	2.6	17		
	15	161.8	1.7	0.92				28	138.2	2.5	15		
	20	159.0	1.55	1.2	2.25	730		28	138.3	2.6	15		
	20	159.8	1.5	1.7				30	*136.4*	*2.0*	*15*		
	25	*160.1*	*1.95*	*1.3*	*2.14*			30	*135.5*	*1.8*	*16*		
5.08	20	149.2	2.4	2.0			15.7	25	139.9	2.5	36		
	20	148.9	2.4	1.4				28	137.5	2.45	27		
	25	148.3	2.1	1.7	1.64	1800		28	137.5	2.6	28		
	25	148.1	2.0	2.1				30	*136.3*	*1.8*	*35*	*1.9*	
	28	*145.2*	*2.6*	*2.0*	*2.97*			30	*135.0*	*1.65*	*43*		

[a] Values in italics are for conditions where gelatin solutions gel in the slow helix growth region ($T_l < T < T_{gel}$).

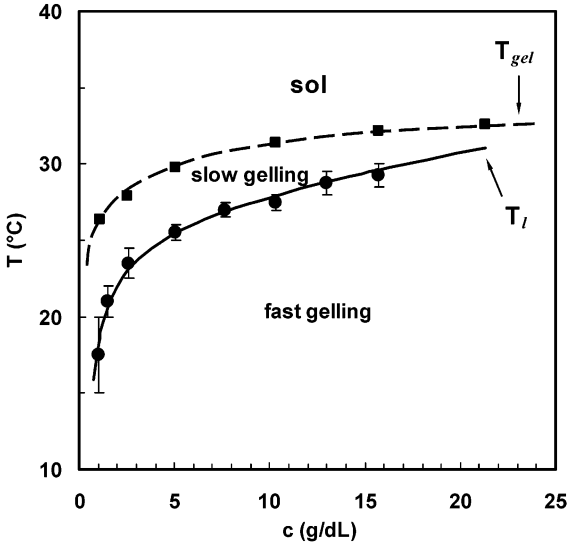

Figure 9. Phase diagram for the fast and slow helix growth regions as well as the sol−gel regions. The sol−gel transition temperature (T_{gel}) data are taken from Michon and coworkers.[16] The dashed line through the T_{gel} data is drawn for visual guidance. The solid line is the fit according to eq 14.

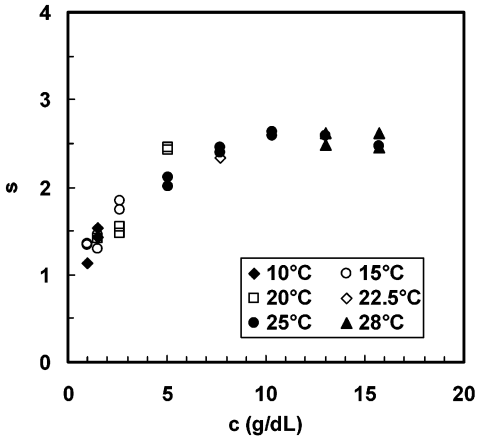

Figure 10. Dynamic scaling exponent *s* determined using the procedure of Figure 8 for the viscosity change ($\Delta\eta$), plotted as a function of gelatin concentration, using only data from the fast helix growth regime.

in the fast helix growth region, where X provides a reliable measure of the bond fraction p. Between T_l and T_{gel}, the gel point occurs beyond the knee of the optical rotation curve, where helix lengthening corrupts the relation between X and p. The slow gelling region gradually diminishes at high concentrations when the T_l line approaches the T_{gel} line.

Figure 10 shows the viscosity exponent *s* as a function of gelatin concentration for all the experimental situations in which the gelatin solution reaches the gel point in the *fast* helix growth region ($T < T_l$). It is clearly seen that the scaling exponent *s* increases with gelatin concentration and saturates above ~10 g/dL. Figure 11 presents the specific viscosity measured at 45 °C as a function of concentration on logarithmic scales. The three usual scaling regimes (dilute, semidilute unentangled, and entangled) for gelatin solutions in the coil state are clearly evident. Below the overlap concentration $c^* \approx 3.5$ g/dL, the solution viscosity is proportional to concentration, indicating dilute solutions where coils rarely interact. Above the entanglement concentration $c_e \approx 12$ g/dL, a power law $\eta \sim c^{3.5}$ is observed, consistent with expectations for entangled polymer solutions. In the intermediate concentration range of ~3.5−12 g/dL, the solution viscosity scales with concentration with an exponent of 2. This value is expected for semidilute, unentangled solutions in a θ-solvent and, for gelatin in water, the Flory−Huggins interaction parameter $\chi = 0.49 \pm 0.01$[44,45] is close to the θ-solvent value of $^1/_2$. *Near the overlap concentration, the viscosity exponent s is in good agreement with the Rouse model prediction of* $s = {}^4/_3$. Comparison of Figures 10 and 11 reveals that the viscosity exponent *s* increases with gelatin concentration in the semidilute, unentangled regime ($c < 12$ g/dL), and saturates at $s \simeq 2.5$ in the entangled regime (c >12 g/dL).

Figure 12 plots the critical helix fraction at the gel point X_{gel} against gelatin concentration for the circumstances where the gelatin solutions gel in the *fast* helix growth region. It is observed that the helix fraction

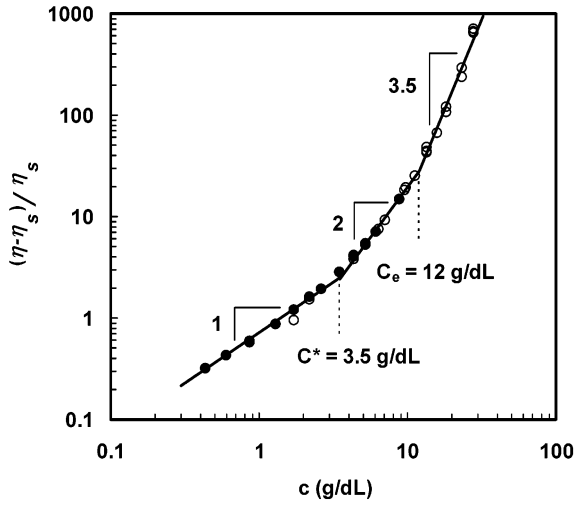

Figure 11. Specific viscosity of gelatin solutions at 45 °C as a function of concentration. Data points in open symbols were measured with a Bohlin CS50 controlled-stress rheometer and data points in filled symbols were determined with an Anton Paar AMVn rolling ball viscometer.

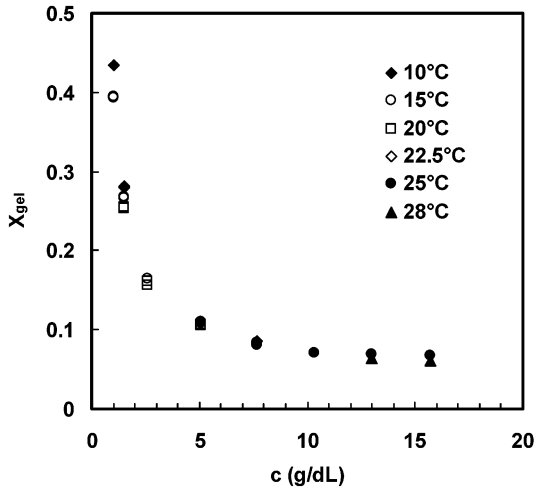

Figure 12. Critical helix fraction at the gel point plotted as a function of gelatin concentration.

required to reach the gel point decreases with concentration and approaches a stable value at high concentrations. One possible explanation of Figure 12 is that a higher fraction of intramolecular cross-links are formed at lower concentration, requiring a higher fraction of helix to reach the gel point. *A constant helix fraction at the gel point for high gelatin concentrations confirms Flory's idea*[46] *that there is a constant cross-link density per polymer chain for the network to be formed.* It is also observed in Figure 12 that the critical helix fraction X_{gel} at the gel point is lowered at higher quench temperatures for which longer and fewer helices are created. This result indicates that helices created at higher temperatures are more efficient in connecting molecules, and therefore, fewer helices are needed to reach the gel point. Since a constant average number of cross-links per molecule is expected at the gel point (Flory's idea[46]), this result, in turn, implies that a larger portion of the total cross-links created at higher temperatures are intermolecular, because intramolecular cross-links do not connect molecules. This is consistent with our separate kinetics study[39] where it is found that intermolecular triple helix formation increasingly dominates over intramolecular helix formation when temperature is raised.

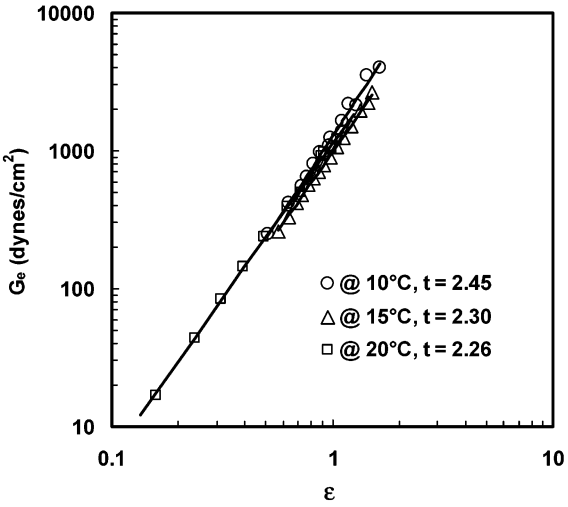

Figure 13. Shear modulus of a 1.51 g/dL gelatin solution at different temperatures fitted to the dynamic scaling prediction $G_e = B\epsilon^t$, with ϵ given by eq 8 and $[\alpha]^{gel}$ determined from viscosity scaling fitting.

Modulus Above the Gel Point. Beyond the gel point, elastic modulus was correlated with optical rotation at different concentrations and temperatures. These data were fit to the scaling prediction of eq 3. Unfortunately, it is not possible to perform a proper creep/recovery experiment very close to the gel point to measure the equilibrium elastic modulus because the relaxation time is too long in the vicinity of the gel point. Consequently, *the gel point determined from viscosity measurements is significantly more accurate than the gel point determined from modulus measurements.* Thus, to test the scaling predictions of eq 3, we use the $[\alpha]^{gel}$ values determined from the viscosity/optical rotation measurements below the gel point in the analysis of the modulus data above the gel point to determine the exponent *t*. Figure 13 shows the result of fitting the modulus for a 1.51 g/dL gelatin solution to eq 3 for three different quench temperatures. These data are described by power laws as expected from dynamic scaling theory, and within experimental uncertainty, the slopes are the same. This was also observed for a 2.62 g/dL gelatin solution quenched to 15, 20, and 25 °C, yielding slopes of $t = 2.16$, 2.25, and 2.14, respectively. Djabourov and co-workers[6] report that $t = 1.82$ for a 4.7 wt % gelatin solution quenched to seven different temperatures in the range from 24 to 28 °C.

Figure 14 shows the modulus data of a 5.08 g/dL gelatin solution quenched to 25 and 28 °C. The data points at different temperatures do not overlap and the power laws have very different exponent values at the two temperatures. Table 2 summarizes the *t* exponents determined at various temperatures and concentrations, with the values in italics obtained in the slow helix growth regime. Figure 15 shows the variation in the modulus exponent *t* as a function of gelatin concentration for the experimental situations where the gel point is in the *fast* helix growth region. At the low concentration end, the measured *t* exponent approaches the value expected by the Rouse model ($t \simeq 2.6$), but *t* decreases as gelatin concentration is raised.

Because of the narrow range of the fast helix growth region and the difficulty in performing creep/recovery measurements close to the gel point, the majority of the

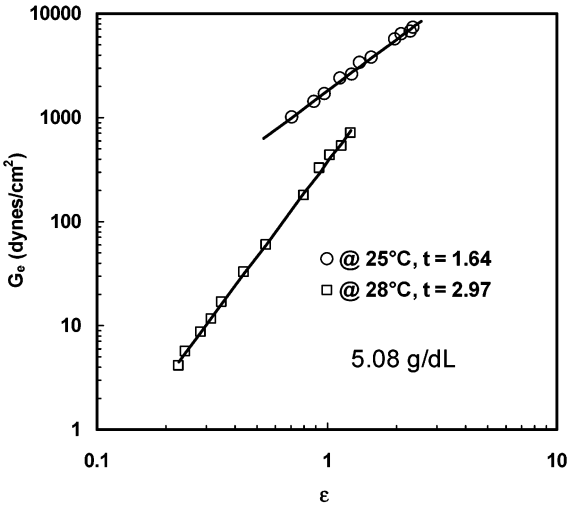

Figure 14. Shear modulus of a 5.08 g/dL gelatin solution at different temperatures fitted to $G_e = B\epsilon^t$, with ϵ given by eq 8, and $[\alpha]^{gel}$ determined by fitting viscosity to $\Delta\eta = A|\epsilon|^{-s}$.

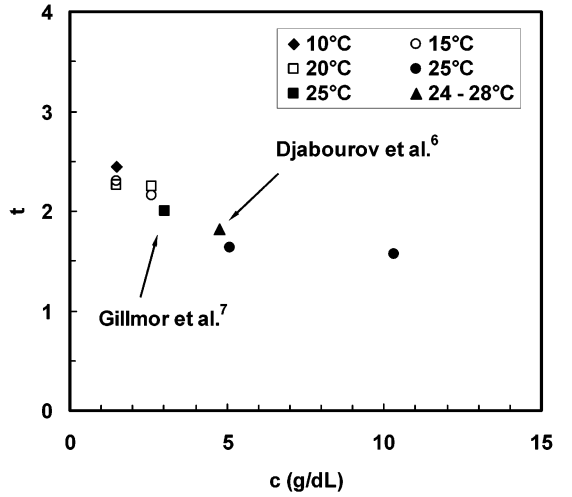

Figure 15. Dynamic scaling exponent t, determined using the procedure of Figures 13 and 14, plotted as a function of gelatin concentration using only data from the fast helix growth regime. Data from Djabourov et al.[6] and Gillmor et al.[7] are also plotted.

modulus data were taken in the slow helix growth region, in contrast to the situation for viscosity measurements where a much broader range of quenching temperatures was explored at each concentration. The experimental situation is frustrating in that accurate modulus measurement close to the gel point is not possible owing to the long relaxation times, and the optical rotation data far beyond the gel point do not accurately reflect the change in bond fraction p. Hence, determination of the exponent t by optical rotation measurements, can only be made with extreme caution.

Relaxation Exponent *u*. In Figure 16, the relaxation exponent u (filled symbols) is plotted together with the ratio $t/(s + t)$ (open symbols) for our gelatin solutions in the fast helix growth region. The filled circles are taken from Michon and co-workers' data[16] that correspond to their lowest measurable temperatures (the fast helix growth region). It is observed that the exponent u and the ratio $t/(s + t)$ coincide when the data are taken in the fast helix growth region. This implies that dynamic scaling (eq 5) is valid for gelatin gelation in the fast helix growth region. The decrease of u with

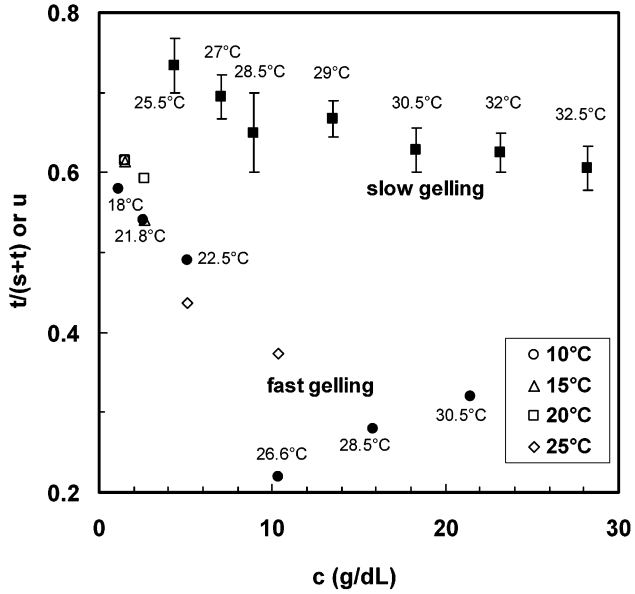

Figure 16. Concentration dependence of the relaxation exponent u and ratio $t/(s + t)$ for gelatin samples. Filled circles are data from Michon and co-workers[16] at the temperatures indicated.

increasing concentration is consistent with results on chemical gelation.[47,48] Lower u at higher concentration may be related to the increased amount of entanglements and cross-link efficiency at higher concentrations, because inefficient cross-linking increases[47] and entanglement lowers[35,47,49] u in chemical gelation without solvent.

Our relaxation exponent u data (filled squares), taken at relatively high temperatures, have significantly higher value than the ratio $t/(s + t)$ that is taken at lower temperatures with the optical rheometry apparatus. The measurements on u were mainly performed in the slow helix growth region, owing to the time required for dynamic measurements (the scaling relation in eq 4 is valid at long relaxation times or low frequencies). Michon and co-workers' u data[16] at high temperatures have similar values to ours. The observed higher u values are believed to be the consequence of the fact that the gelatin solutions reach the gel point in the slow helix growth region at these high temperatures. Michon and co-workers have measured the exponent u over a wide range of temperatures for several gelatin concentrations. The exponent u is found to increase with temperature and levels off when T_{gel} is approached. This same trend of u increasing with temperature is also observed for thermal physical gelation of isotactic polypropylene.[50]

Conclusions

Upon cooling, gelatin undergoes physical gelation by forming triple helices. The fraction of gelatin in the helix state is readily monitored by optical rotation with high precision. There are two helix formation processes that depend on temperature and concentration, which must be considered when interpreting results: helix creation and helix lengthening. Only in the *fast* gelling regime, at a temperature lower than T_l, does a simple relation exist between optical rotation and cross-link density. Thus, it is only in this regime where scaling theories can be easily tested. Effective exponents determined in the slow gelling regime are difficult to interpret physi-

cally. These findings partially explain the wide range of rheological exponents reported from applying scaling ideas to physical gelation of gelatin. Much of the literature data were obtained in the slow gelling regime (with $T > T_l$) where helix lengthening precludes the use of optical rotation to determine the extent of cross-linking.

For gelatin gels formed in the fast gelling regime (with $T < T_l$), the rheological exponents depend on concentration, but not on temperature. The exponent for the viscosity increases with concentration, from the Rouse model prediction of $s \simeq 1.3$ near the overlap concentration to $s \simeq 2.5$ for entangled gelatin solutions. The exponent t describing the growth of modulus beyond the gel point decreases with concentration from the Rouse model prediction of $t \simeq 2.6$ near the overlap concentration to $t \simeq 1.6$ for entangled gelatin solutions. The relaxation exponent u obeys the dynamic scaling law $u = t/(s + t)$, making u decrease as concentration is raised, from $u \approx 0.6$ near the overlap concentration to $u \approx 0.3$ for entangled solutions. These concentration dependences of rheological exponents are consistent with literature observations for both physical and chemical gels. However, more theoretical work is needed to fully understand these concentration dependences, and in particular, no theory predicts the exponent values observed in the entangled regime.

Since the relation $u = t/(s + t)$ is valid for our gelatin system, the longest relaxation time below the gel point, $\lambda^-_{max} \propto (-\epsilon)^{-s/(1-u)}$, and the longest relaxation time above the gel point, $\lambda^+_{max} \propto \epsilon^{-t/u}$, are symmetric at the gel point, leading to an identical relaxation time exponent, $s/(1 - u) = t/u = s + t$. Our results further suggest that the relaxation time exponent $s + t$ is concentration independent with a value of ~4.

Our results call for a reexamination of all the reported rheological exponents measured on physical gels, because the nature of the association may change over the gelation process. For gelatin, helix lengthening occurs at long times at every temperature and concentration. Similar structural changes may occur in other physical gelling systems. Caution is needed in interpreting the rheological exponents measured in systems undergoing physical gelation.

Acknowledgment. We thank Eastman Kodak Co. for financial support of this research, and thank Gerry Fuller, Tom Whitesides, Jeff Gillmor, Julia Tan, Roland Koestner, and Rich Connelly for interesting technical discussions.

Appendix I

The photoelastic modulator in the optical train setup displayed in Figure 2 modulates retardation $R(t)$ by oscillating at a specified frequency Ω,

$$R(t) = R_0 \cos \Omega t \tag{15}$$

where $R_0/2\pi$ is the maximum retardation expressed as number of waves of the light beam. We can always start counting at a particular time to neglect the initial phase angle in eq 15. The modulator only affects the polarized light component that is parallel to its axis, while the component perpendicular to the axis is not modulated. For the optical train in Figure 2, the modulator axis is parallel to the polarized beam direction pointing out of the paper, which is defined as the x-axis of the reference coordinates. The perpendicular direction downward is defined as the y-axis, and the light propagation direction is defined as the z-axis. The first polarizer is along the x-axis, while the second polarizer is at a 45° angle to the x-axis, either positive or negative, depending on the optical rotation direction to make the measurement most sensitive.

The electric field of the polarized light wave after the first polarizer can be described as an oscillating function of distance z and time t

$$A_x = A_0 \cos(kz - \omega t + \beta) \tag{16}$$

where A_0 is the amplitude, $k = 2\pi/\lambda$ is the wavenumber, λ and ω ($\gg\Omega$) are the wavelength and frequency of the light, and β is the phase difference from the photoelastic modulator. The polarized beam is rotated an angle of α after passing through the sample and the two components of the light become

$$A_x^\alpha = A_0 \cos \alpha \cos(kz - \omega t + \beta)$$
$$A_y^\alpha = A_0 \sin \alpha \cos(kz - \omega t + \beta) \tag{17}$$

After the modulator, the component A_y^α remains unchanged while A_x^α is modulated with a constantly changing retardation, and the two new components are

$$A_x^{PEM} = A_0 \cos \alpha \cos(kz - \omega t + \beta + R(t))$$
$$A_y^{PEM} = A_0 \sin \alpha \cos(kz - \omega t + \beta) \tag{18}$$

The second polarizer (analyzer) is placed ±45° relative to the x-axis; thus, after the analyzer, the combined wave function along the analyzer axis will be

$$\begin{aligned} A^* &= \frac{1}{\sqrt{2}}(A_x^{PEM} \pm A_y^{PEM}) \\ &= \frac{A_0}{\sqrt{2}}[\cos \alpha \cos(kz - \omega t + \beta + R(t)) \pm \\ &\qquad \sin \alpha \cos(kz - \omega t + \beta)] \\ &= \frac{A_0\sqrt{1 \pm \sin 2\alpha \cos R(t)}}{\sqrt{2}} \cos(kz - \omega t + \beta + \gamma) \end{aligned} \tag{19}$$

where γ satisfies

$$\sin \gamma = \frac{\cos \alpha \sin R(t)}{\sqrt{1 \pm \sin 2\alpha \cos R(t)}} \tag{20}$$

Since the frequency $\omega(\gg \Omega)$of the light is too high for the detector to respond, the term $\cos(kz - \omega t + \beta + \gamma)$ in the wave function eq 19 will produce a constant intensity on the detector. However, the detector can respond to the change in the relatively low frequency Ω, and the intensity measured on the detector is

$$I \propto \frac{{A_0}^2}{2}(1 \pm \sin 2\alpha \cos R(t)) \tag{21}$$

Substituting the Fourier expansion of the retardation function

$$\cos R(t) = B_0 + B_1 \cos \Omega t + B_2 \cos 2\Omega t + \ldots \tag{22}$$

in eq 21 leads to

$$I \propto \frac{A_0^2}{2}(1 \pm B_0 \sin 2\alpha \pm B_1 \sin 2\alpha \cos \Omega t \pm B_2 \sin 2\alpha \cos 2\Omega t + ...) \quad (23)$$

Hence, the amplitude ratio of the 2Ω component to the dc component is

$$\frac{V_{2\Omega}}{V_{dc}} = \left|\frac{B_2 \sin 2\alpha}{1 \pm B_0 \sin 2\alpha}\right| \quad (24)$$

The two constants B_0 and B_2 are determined by calibration and the orientation of the analyzer (±45°) sets the sign in eq 24 and delivers different sensitivities for the measurement. The intensity as expressed in eq 21 may fluctuate with time, but the ratio $V_{2\Omega}/V_{dc}$ does not. Using the ratio ensures a sensitive and accurate measurement of optical rotation.

Appendix II

The obvious choice for the helix creation rate is the time derivative of the molar helix concentration. Our kinetics study[39] has shown that the helix formation process in gelatin solutions is a combined coil−helix reversion of the first- and second-order concentration dependences. The first-order reversion corresponds to intramolecular cross-linking and does not contribute to network formation (or gelation). *Primarily, the second-order reversion corresponds to intermolecular cross-linking and is the process responsible for gelation.* The second-order helix formation rate during the initial stage of quenching can be expressed as[39]

$$\frac{d[H]_2}{dt} \sim c_0^2 \exp\left(-\mu \frac{T_m^0}{\Delta T}\right) \quad (25)$$

where $[H]_2$ is the second-order molar density of helices, c_0 is the initial gelatin concentration, and μ is a constant. For all the cases where the knee position on the optical rotation curve coincides with the gel point, we expect that the helix creation rate at different concentrations is identical; thus, the right side of eq 25 is constant

$$c_0^2 \exp\left(-\mu \frac{T_m^0}{T_m^0 - T_l}\right) = \exp(F) \quad (26)$$

Rearranging eq 26 leads to the expression for T_l:

$$T_l = T_m^0\left(1 - \frac{\mu}{2\ln c_0 - F}\right) \quad (27)$$

The concentration-dependent equilibrium melting temperature T_m^0 can be described by a simple linear relation[39] through reanalyzing Godard and co-workers' data[51]

$$T_m^0(°C) = 35 + 0.18c_0 \quad (28)$$

with c_0 in g/dL.

Our kinetics study[39] shows that $\mu = 0.28$ for our gelatin system. Remelting analysis of the present study finds that 25 °C < T_l < 28 °C for a 5.08 g/dL solution. From Table 2, 7.68 and 10.3 g/dL solutions have T_l values in the range from 25 to 28 °C. Consequently, $T_l = 25.5 \pm 0.5$ °C for the 5.08 g/dL solution is a convenient reference, and we calculate the constant F in eq 27 accordingly. The final result is as follows, with temperature in Kelvin:

$$T_l(K) = (35 + 0.18c_0 + 273)\left(1 - \frac{0.28}{2\ln c_0 + 5.06}\right) \quad (29)$$

References and Notes

(1) Ferry, J. D.; Eldridge, J. E. *J. Phys. Chem.* **1949**, *53*, 184.
(2) Flory, P. J.; Weaver, E. S. *J. Am. Chem. Soc.* **1960**, *82*, 4518.
(3) Harrington, W. F.; Rao, N. V. *Biochemistry* **1970**, *9*, 3714.
(4) Djabourov, M. *Contemp. Phys.* **1988**, *29*, 273.
(5) Djabourov, M.; Leblond, J.; Papon, P. *J. Phys. (Paris)* **1988**, *49*, 319.
(6) Djabourov, M.; Leblond, J.; Papon, P. *J. Phys. (Paris)* **1988**, *49*, 333.
(7) Gillmor, J. R.; Connelly, R. W.; Colby, R. H.; Tan, J. S. *J. Polym. Sci., Part B, Polym. Phys.* **1999**, *37*, 2287.
(8) Ramachandran, G. N.; Kartha, G. *Nature (London)* **1954**, *174*, 269 and **1955**, *176*, 593.
(9) Pezron, I.; Djabourov, M.; Bosio, L.; Leblond, J. *J. Polym. Sci., Part B: Polym. Phys.* **1990**, *28*, 1823.
(10) Pezron, I.; Herning, T.; Djabourov, M.; Leblond, J. In *Physical Networks*; Burchard, W, Ross-Murphy, S. B., Eds.; Elsevier: Amsterdam, 1990.
(11) Djabourov, M.; Bonnet, N.; Kaplan, H.; Favard, N.; Favard, P.; Lechaire, J. P.; Maillard, M. *J. Phys. II (Paris)* **1993**, *3*, 611.
(12) Horský, J.; Švantner, J. *Polym. Int.*, **1993**, *32*, 159.
(13) Stauffer, D.; Aharony, A. *Introduction to Percolation Theory*; 2nd ed.; Taylor and Francis: London, 1992.
(14) Djabourov, M. *Polym. Int.* **1991**, *25*, 135.
(15) Axelos, M. A. V.; Kolb, M. *Phys. Rev. Lett.* **1990**, *64*, 1457.
(16) Michon, C.; Cuvelier, G.; Launay, B. *Rheol. Acta* **1993**, *32*, 94.
(17) Hsu, S.; Jamieson, A. M. *Polymer* **1993**, *34*, 2602.
(18) Chambon, F.; Winter, H. H. *Polym. Bull. (Berlin)***1985**, *13*, 499.
(19) Winter, H. H.; Chambon, F. *J. Rheol.* **1986**, *30*, 367.
(20) Chambon, F.; Winter, H. H. *J. Rheol.* **1987**, *31*, 683.
(21) Martin, J. E.; Adolf, D.; Wilcoxon, J. P. *Phys. Rev. Lett.* **1988**, *61*, 2620; *Phys. Rev. A* **1989**, *39*, 1325.
(22) Colby, R. H.; Gillmor, J. R.; Rubinstein, M. *Phys. Rev. E* **1993**, *48*, 3712.
(23) Durand, D.; Delsanti, M.; Adam, M.; Luck, J. M. *Europhys. Lett.* **1987**, *3*, 297.
(24) Stauffer, D.; Coniglio, A.; Adam, M. *Adv. Polym. Sci.* **1982**, *44*, 103.
(25) Flory, P. J. *J. Am. Chem. Soc.* **1941**, *63*, 3083.
(26) Stockmayer, W. H. *J. Chem. Phys.* **1943**, *11*, 45.
(27) De Gennes, P. G. *Scaling Concepts in Polymer Physics*; Cornell University Press: Ithaca, NY, 1979.
(28) Adolf, D.; Martin, J. E.; Wilcoxon, J. P. *Macromolecules* **1990**, *23*, 527.
(29) Rubinstein, M.; Colby, R. H.; Gillmor, J. R. *Polym. Prepr. (Am. Chem. Soc., Div. Polym. Chem.)* **1989**, *30*, 81. In *Space-Time Organization in Macromolecular Fluids*; Tanaka, F.; Doi, M.; Ohta, T., Eds.; Springer-Verlag: Berlin, 1989.
(30) Kantor, Y.; Webman, I. *Phys. Rev. Lett.* **1984**, *52*, 1891.
(31) Hodgson, D. F.; Amis, E. J. *Macromolecules* **1990**, *23*, 2512.
(32) Colby, R. H.; Coltrain, B. K.; Salva, J. M.; Melpolder, S. M. In *Fractal Aspects of Materials: Disordered Systems*; Hurd, A. J., Weitz, D. A., Mandelbrot, B. B., Eds.; Materials Research Society: Pittsburgh, PA, 1987.
(33) Lairez, D.; Adam, M.; Emery, J. R.; Durand, D. *Macromolecules* **1992**, *25*, 286.
(34) Lusignan, C. P.; Mourey, T. H.; Wilson, J. C.; Colby, R. H. *Phys. Rev. E* **1995**, *52*, 6271.
(35) Lusignan, C. P.; Mourey, T. H.; Wilson, J. C.; Colby, R. H. *Phys. Rev. E* **1999**, *60*, 5657.
(36) (a) Li, L.; Aoki, Y. *Macromolecules* **1997**, *30*, 7835. (b) Li, L.; Uchida, H.; Aoki, Y.; Yao, M. L. *Macromolecules* **1997**, *30*, 7842.
(37) Hauschka, P. V.; Harrington, W. F. *Biochemistry* **1970**, *9*, 3734.
(38) Von Hippel, P. H.; Wong, K. Y. *Biochemistry* **1963**, *2*, 1399.
(39) Guo, L.; Colby, R. H.; Lusignan, C. P.; Whitesides, T. H. *Macromolecules* **2003**, *36*, 9999.
(40) *PEM-90 Photoelastic Modulator Systems User Manual*; Hinds Instruments, Inc.: Hillsboro, OR, 1996.

(41) Fuller, G. G. *Optical Rheometry of Complex Fluids*; Oxford University Press: New York, 1995.
(42) Winter, H. H.; Mours, M. *Adv. Polym. Sci.* **1997**, *134*, 165.
(43) Huang, H.; Sorensen, C. M. *Phys. Rev. E* **1996**, *53*, 5075.
(44) Pezron, I.; Djabourov, M.; Leblond, J. *Polymer* **1991**, *32*, 3201.
(45) Bohidar, H. B.; Jena, S. S. *J. Chem. Phys.* **1994**, *100*, 6888.
(46) Flory, P. J. *Principles of Polymer Chemistry*; Cornell University Press: Ithaca, NY, 1953.
(47) Scanlan, J. C.; Winter, H. H. *Macromolecules* **1991**, *24*, 47.
(48) Kjøniksen, A.-L.; Nyström, B. *Macromolecules* **1996**, *29*, 5215.
(49) Gasilova, E.; Benyahia, L.; Durand, D.; Nicolai, T. *Macromolecules* **2002**, *35*, 141.
(50) Pogodina, N. V.; Winter, H. H. *Macromolecules* **1998**, *31*, 8164.
(51) Godard, P.; Biebuyck, J. J.; Daumerie, M.; Naveau, H.; Mercier, J. P. *J. Polym. Sci.: Polym. Phys. Ed.* **1978**, *16*, 1817.

MA034266C